Unraveling the Nature of Turkevich Gold Nanoparticles: The Unexpected Role of the Dicarboxyketone Species

Daniel Grasseschi, Rômulo A. Ando, Henrique E. Toma, Vitor M. Zamarion *

*corresponding author: zamarion@iq.usp.br

Support Information

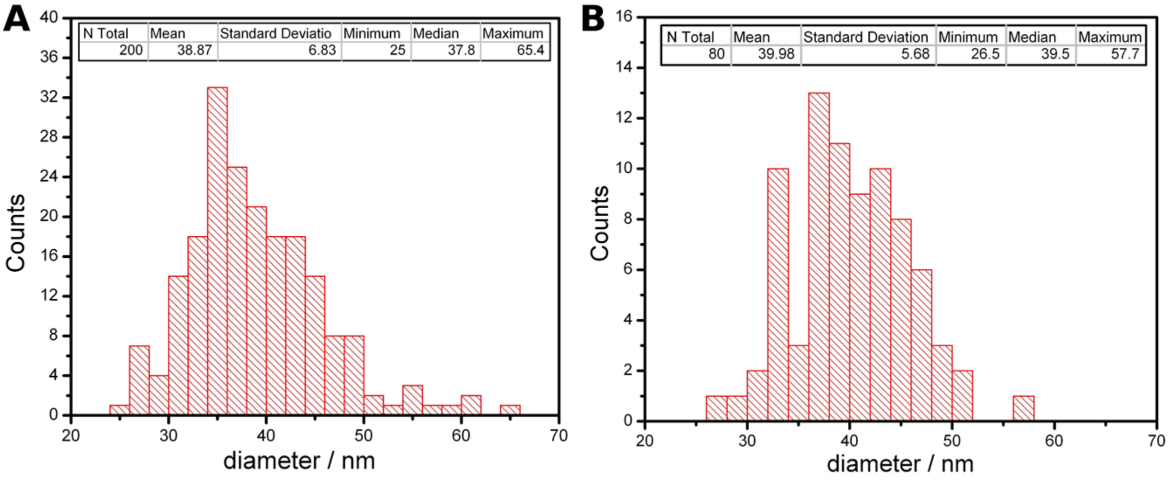

Figure S 1 - Histogram for size distributions: cit-AuNP (A) and ket-AuNP (B).

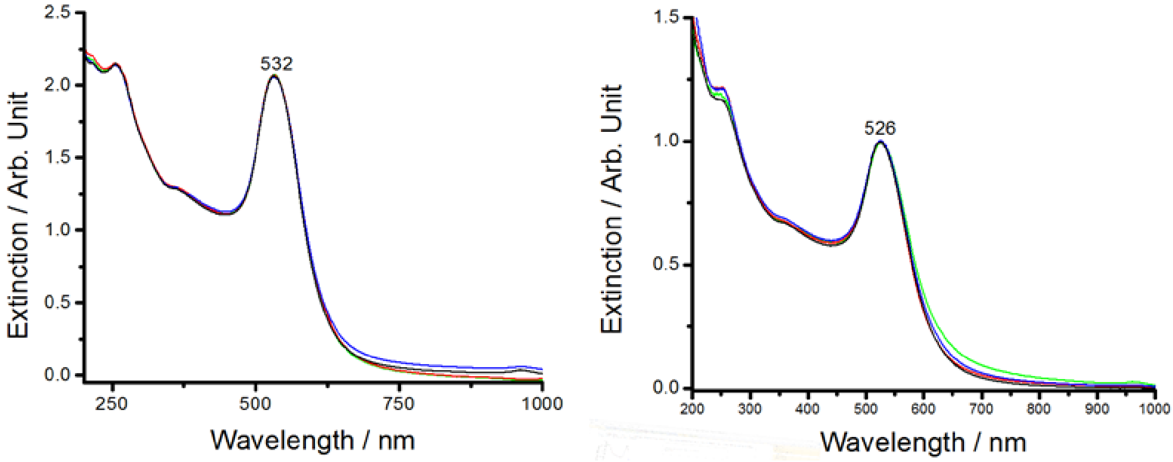

Figure S 2. Extinction spectra of ket-AuNP (left) and cit-AuNP (right), for several synthesis.

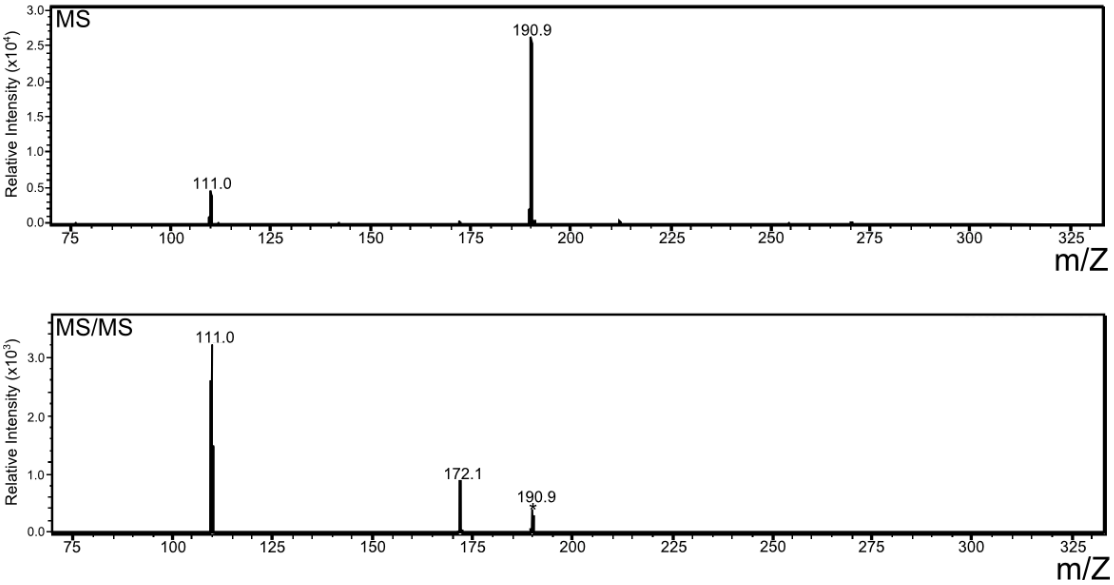

Figure S 3. MS/MS spectrum of sodium citrate. The mas in 190.9 correspond to citrate.

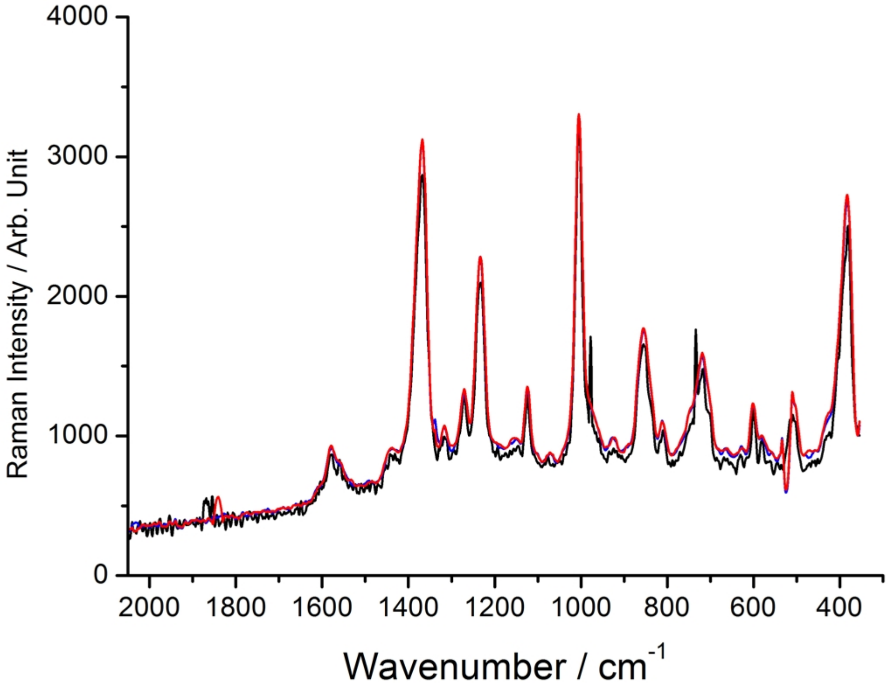

Figure S 4. SERS spectra of ket-AuNP, for several synthesis.

For 1,3-dicarbonyl compounds, like dicarboxyketone, it is common to see thermodynamically stable enols, due to electronic delocalization between the two carbonyl groups and the formation of intramolecular hydrogen bond forming a six member ring.[1] Then, assuming the possibility of coordination not only by the oxygen, in the ketone form, but also, by the carbon in the enol form, we performed theoretical calculations for dicarboxyketone/enol assuming more than one conformation. Since citrate does not have this type of equilibrium, the calculation was performed for one structure only.

Figure S 5 shows some possible dicarboxyenol conformations. The frontier orbitals show that depending on the degree of distortion and the H-bond strength, the enolic molecular structure has the HOMO located at the carbon atoms from the double bond, while LUMO is located at the C-O bonds. In the case of a distorted structure where there is no H-bond in the 6 membered ring, the HOMO is centered mainly on the ring oxygens. Thus, charge controlled interactions will occur mainly in the oxygens and have a hard character, e.g. the complex formation with rare earth. While, the interaction with soft-acid, like the gold atoms, should be governed by the frontier orbital occurring in the C=C bond of the enol form. These findings are important to attribute the molecular disposition at the surface.

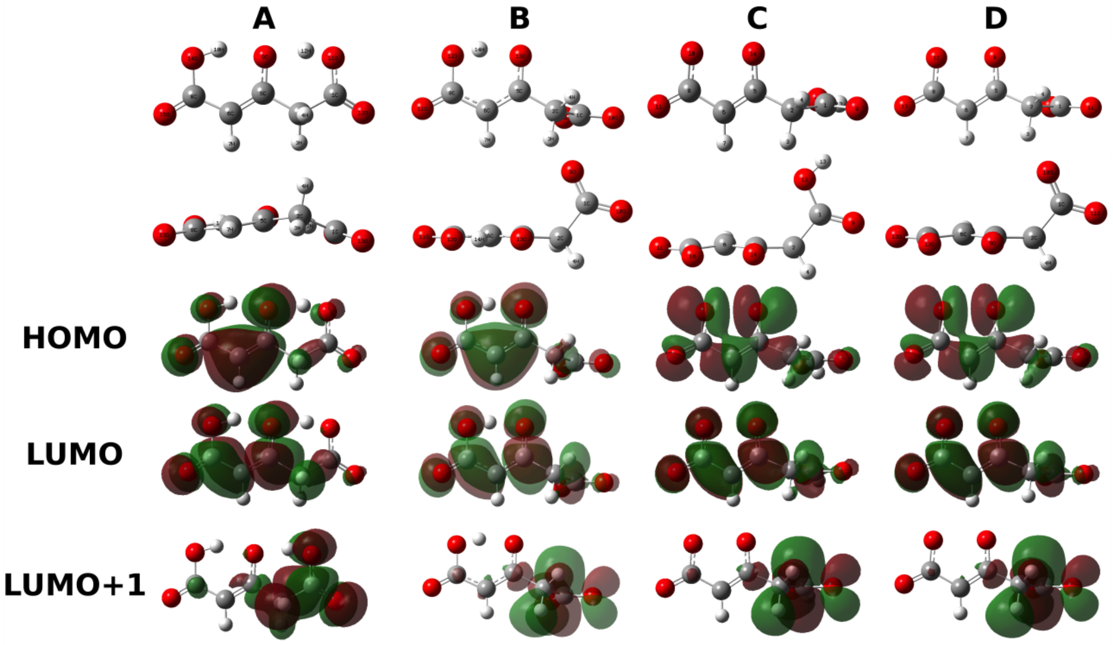

Figure S 5. Frontier orbitals of different conformations of dicarboxyenol molecules.

For a better visualization and data interpretation, Figure S 6 shows the theoretical spectra of possible stable conformations of dicarboxyketone molecule and the SERS spectrum of ket-AuNPs, highlighting the resemblance between each species. So, aiming a lower computational cost, the molecules alone were studied deeply before gold was introduced into the calculations.

In addition, Figure S 7 shows the SERS spectra of ket-AuNPs in extreme pH values; where besides a better understanding of bands assignment it’s possible to disregard the possibility of only an acid-base equilibrium of citrate for surface coordination.

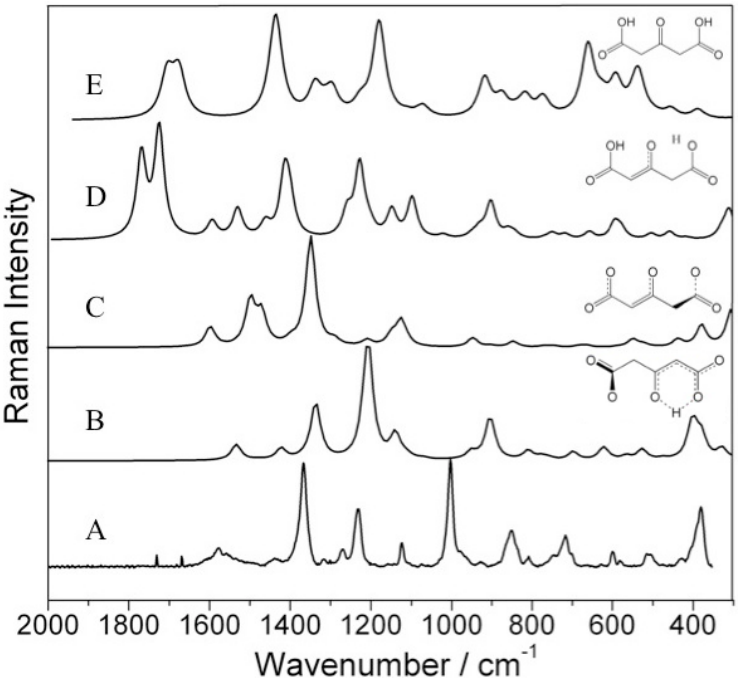

Figure S 6. Comparison between experimental SERS spectrum of ket-AuNP (A) and theoretical Raman spectra of dicarboxyenol/ dicarboxyketone: B) Dicarboxyenol distorted in one of the carboxylates and doubly deprotonated; C) Dicarboxyenol distorted in one of the carboxylates and deprotonated; D) Planar dicarboxyenol; E) Dicarboxyketone.

To first assign which molecule is in fact bonded to the surface it was performed several calculations of ketone and enol species, considering all acid-base possible equilibria. The theoretical spectra show several differences when the molecules are deprotonated and distorted, reflecting preferential contributions in the vibration normal modes due to the degree of electron delocalization. Contrasting all information obtained, it is more likely that a mixture of species can be found in surface with the planar and distorted forms, together. The planar and distorted forms can be seen in Figure S 5 labeled as structure A and B, respectively.

Table 1 and Table S1 shows a comparison between SERS spectra of ket-AuNPs, the theoretical spectra of deprotonated planar dicarboxyenol and the dicarboxyenol distorted in one of the carboxylates and doubly deprotonated. As already mentioned, the electronic delocalization is highlighted by the shifts and the different band intensities.

For example, the theoretical spectrum of the distorted form has one band in 1592 cm^{-1}, attributed to $\nu O^{10}C^{1}O^{11}_{ass}$. The planar form, otherwise, presents two theoretical bands in the same region, 1590 cm^{-1}, attributed to $\delta O^{11}H^{12}_{ip} + \nu C^{5}=C^{6}(w)$ and 1527 cm^{-1}, to $\nu C^{5}=C^{6} + 2(\delta O^{11,14}H^{12,10})_{ip}$. The experimental spectrum, however, has a broad band with two maxima in 1579 cm^{-1} and 1557 cm^{-1}, which could at first, be naturally assigned to a mixture of species. Nevertheless, the atoms involved in the vibrations are quite different, with a higher contribution of OH in plane deformation for the planar form and CO stretching for the distorted one. To solve this issue and to proper assign the band, the spectra in different pHs were very helpful.

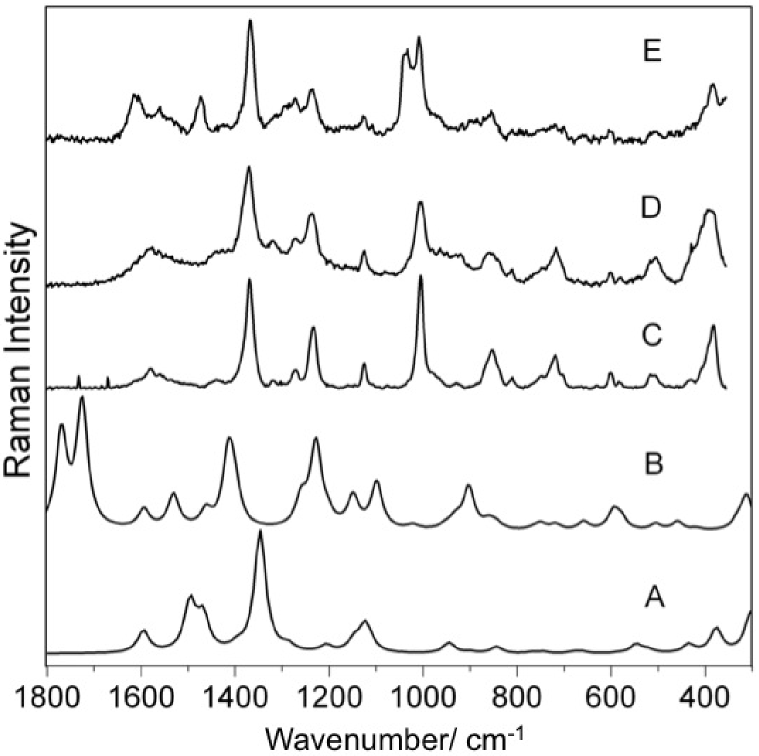

Figure S 7. Comparison between theoretical Raman spectra and Experimental SERS spectra: A) dicarboxyenol distorted in one of the carboxylates and doubly deprotonated, B) planar dicarboxyenol, C) SERS of ket-AuNPs, D) SERS of ket-AuNPs in pH 12 and E) SERS of ket-AuNPs pH 2.5

Looking closely to Figure S 7, two bands can be easily seen in 1609 and 1557 cm^{-1} with a shoulder in 1530 cm^{-1} for pH 2.5, while in pH 12 there is only a broad band. These bands may be a good indicative to assign the spectra in different pH, because in certain way they can distinguish the contributions of both structures for the overall spectra (Figure S 7C). Therefore, we can see more of a planar structure at pH 2.5 and more of a distorted one at pH 12. Additionally, the lower intensity of the mode in 398 cm^{-1} and the rise of the peak on 1470 cm^{-1} are consistent with the presence of the enol under a planar conformation in lower pH values for ket-AuNPs. On the other hand, looking at the SERS spectra on pH 12, these changes on the ket-AuNP SERS spectrum cannot be seen, which indicates that a planar conformation is present in larger quantities in an acidic medium, while more basic conditions favors the distorted enol form.

The experimental spectra in different pH also helped to assign the band around 1000 cm^{-1} of the experimental spectra. The high intensity of this band, according to Table S 1 suggests that the coordination through the C=C bond had in fact happened and the intensity is a conjunction of three factors: a simple C-C bond character[2], the localization of the HOMO centered at C-C atoms and the proximity with the gold surface.

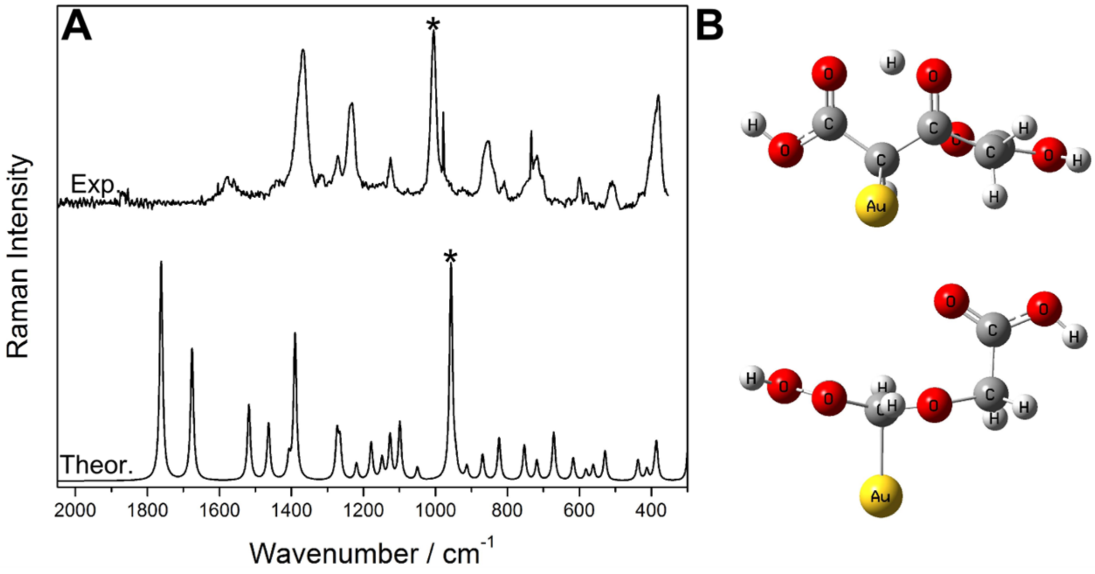

Figure S 8. A) Theoretical Raman, bottom, and SERS spectra, top, of Au-enol system. B) Optimized geometry of Au-dicarboxyenol structure.

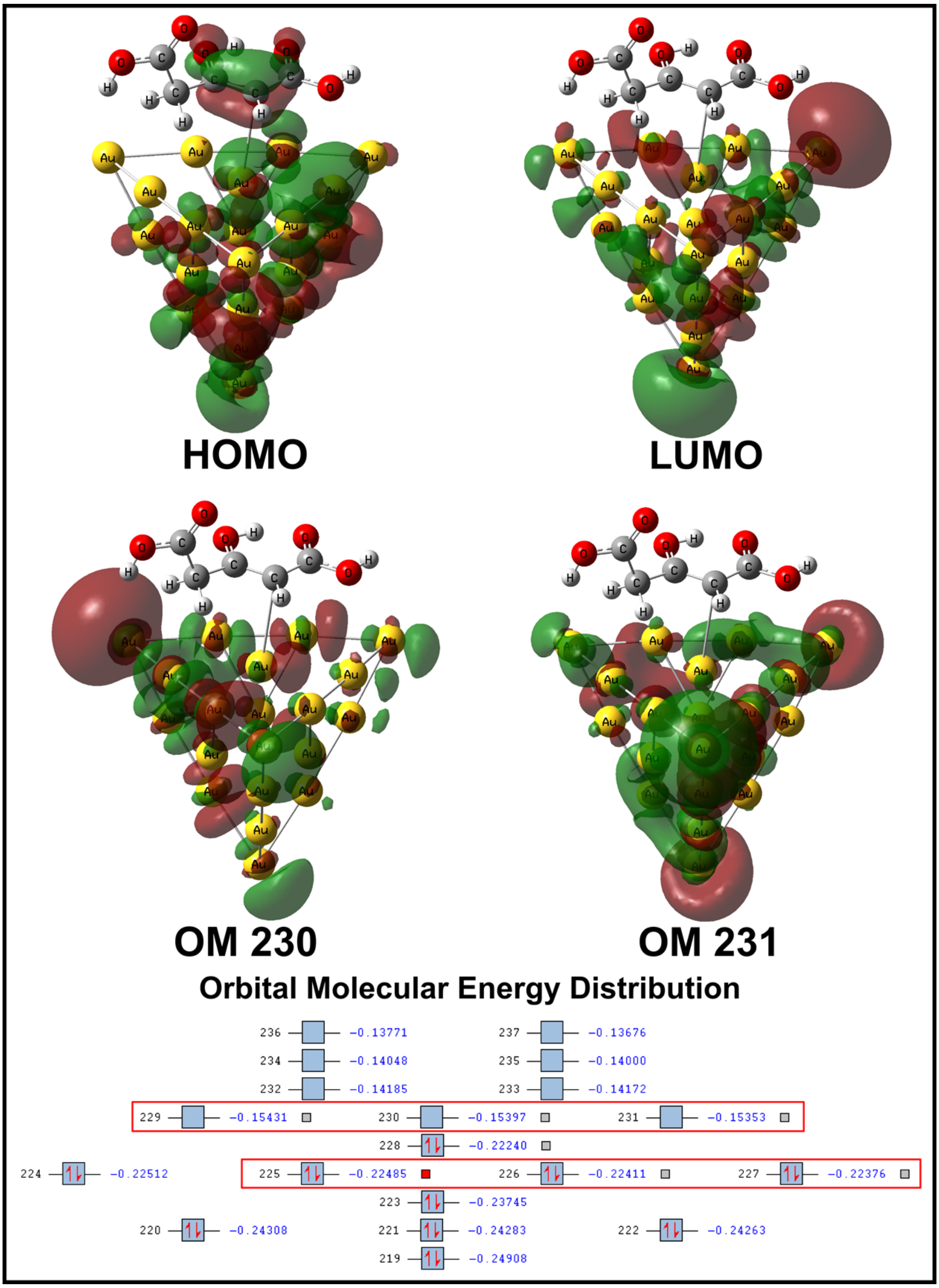

Figure S 9. Representation of the molecular orbitals 230 and 230 involved in the LMCT transition, and the molecular orbital energy distribution.

Table S1. Complete assignment of all possible acid-base equilibria of dicarboxyketone molecule based on Figure 4.

Structure A	Structure B	Structure C	Structure D	Assignment
1764	-	-	-	$\nu C^{1}{=}O^{13} + \delta C^{1}O^{12}H^{13}{}_{ip}$
-	-	1728 (m)	-	$\nu C^{1}{=}O^{9} + \delta O^{14}H^{10}{}_{ip}$(vs)
1722	-	-	-	$\nu C^{8}{=}O^{15}$ (vs) + $\delta O^{14}H^{10}{}_{ip}$
-	-	1676 (vs)	-	$\nu C^{8}{=}O^{11}$ (vs) + $\delta C^{8}O^{10}H^{15}{}_{ip}$(vs)
1590	-	-	-	$\delta O^{11}H^{12}{}_{ip} + \nu C^{5}{=}C^{6}$(w)
-	-		1592	$\nu O^{10}C^{1}O^{11}{}_{ass}$
1527	-		-	$\nu C^{5}{=}C^{6} + 2(\delta O^{11,14}H^{12,10})_{ip}$
-	1530		-	$\nu C^{5}{=}C^{6} + \nu C^{8}\text{-}O^{11}$
-	-		1492	$\nu C^{5}{=}C^{6} + \nu C^{8}\text{-}O^{13} + \delta C^{6}H^{7}$
-	-		1469	$\nu C^{8}\text{-}O^{13} + \nu C^{5}{=}C^{6} + CH_{2}$sci(w)
		1468 (s)		$\delta O^{10}H^{15}{}_{ip}$ (vs) + $\nu O^{10}C^{8}C^{11}$ass
1458	-		-	$\nu C^{8}{=}O^{15}$ (vw) + $\delta O^{14}H^{10}$
-	1418		-	$\nu C^{1}{=}O^{9} + \delta C^{1}O^{12}H^{13} + \delta C^{1}C^{2}H^{4}$
1411	-		-	CH_{2}sci + $\nu C^{6}\text{-}C^{8} + \delta C^{5}C^{6}H^{7} + \nu C^{5}\text{-}C^{9}$
-	-		1392	CH_{2}sci
-	-		1345	$\delta C^{5}C^{6}H^{7} + CH_{2}$twist
-	1334		-	CH_{2}sci + $\nu C^{5}\text{-}O^{14} + \delta C^{5}C^{6}H^{7} + \nu C^{6}\text{-}C^{8}$
-	-		1291	$\delta O^{11}C^{1}O^{10} + \nu C^{1}\text{-}C^{2}$
1256	-		-	CH_{2}wagg + $\delta C^{8}C^{6}H^{7}$ (vw)
1225	-		-	$2(\nu C^{1,8}\text{-}O^{11,14}) + 2(\nu C^{1,6}\text{-}C^{2,8}) + 2CH_{2}$wagg + $\delta O^{14,11}H^{10,12}$
-	1206		-	CH_{2}wagg
-	-		1206	CH_{2}wagg + $\nu C^{6}\text{-}C^{8} + \nu C^{8}\text{-}O^{10}$
-	1137		-	CH_{2}twist + $\delta O^{12}H^{13}$
1145			1145	CH_{2}twist
			1122	$\nu C^{8}{=}O^{12} + \nu C^{5}\text{-}O^{9} + \nu C^{6}\text{-}C^{8} + CH_{2}$twist
	1109			CH_{2}twist + $\delta C^{5}C^{6}H^{7}$
1096				$\delta C^{8}C^{6}H^{7} + CH_{2}$twist
1019				$\delta O^{11}H^{12}{}_{op}$
949				$\nu C^{2}\text{-}C^{5} + 2(\nu C^{5,8}\text{-}O^{9,14}) + CH_{2}$rock (vw)
	949			$\nu C^{2}\text{-}C^{5} + 2(\nu C^{5,8}\text{-}O^{14,10}) + CH_{2}$rock (vw) + $\delta C^{6}C^{5}O^{14}$

			944	$\nu C^{2}\text{-}C^{5} + \nu C^{6}\text{-}C^{8} + CH_{2}$rock
930				$2\nu C^{5,8}\text{-}O^{9,14} + CH_{2}$rock (s)
		928 (vw)		$\delta O^{10}H^{15}{}_{op}$ (vw)
		921 (m)		$(\delta C^{1}C^{2}C^{5} + \delta C^{5}C^{6}C^{8})_{iph} + \nu C^{8}\text{-}O^{10}$
	901			CH_{2}rock $+ \delta O^{12}H^{13}{}_{ip}$
902				CH_{2}rock $+ \nu C^{8}\text{-}O^{14} + \delta C^{2}C^{5}C^{6}$
855				$\nu C^{1}\text{-}C^{2} + \nu C^{8}\text{-}O^{14} + \nu C^{1}\text{-}O^{11} + \delta O^{13}C^{1}O^{11}$
	844			$\delta C^{5}C^{2}C^{1}{}_{op}$ (s) $+\delta C^{8}C^{5}{=}C^{6}{}_{op}$ (w)
			844	$\nu C^{1}\text{-}C^{2} + \delta O^{11}C^{1}O^{10} + \delta C^{2}C^{5}{=}C^{6}{}_{op}$
	807			CH_{2}rock $+ \delta O^{12}H^{13}{}_{ip}$
	776			$\delta C^{8}C^{5}{=}C^{6} + \delta O^{12}H^{13}{}_{ip}$
			768	δlong chain $_{oph,\ op}$
	758			δlong chain $_{ip} + \delta O^{12}H^{13}{}_{ip}$
751				δlong chain $_{ip} + \delta O^{11}H^{12}{}_{ip} + \delta O^{14}H^{10}{}_{op}$
			744	δlong chain $_{iph,\ op}$
720				$\delta C^{6}H^{7}{}_{op} + \delta$ ring
	696			δlong chain $_{op}$
			680	$\delta C^{6}H^{7}{}_{op}$
			662	δlong chain$_{ip} + \delta O^{12}C^{8}O^{13}{}_{ip}$
657				$\delta O^{14}C^{8}O^{15}{}_{ip} + \delta O^{13}C^{1}O^{11}{}_{ip} + \delta O^{6}{=}C^{5}C^{2}{}_{ip}$
		649 (w)		$\delta O^{11}{=}C^{8}O^{10} + \delta O^{12}C^{1}{=}O^{9}$
	620			$\delta O^{10}C^{8}O^{11}{}_{ip} + \nu C^{1}\text{-}C^{2} + \delta O^{12}H^{13}{}_{ip}$
	602			$\delta C^{6}H^{7}{}_{op}$
591				δlong chain$_{op} + CH_{2}$twist
			584	CH_{2}rock $+ \delta O^{9}C^{5}C_{op} + \delta O^{10}C^{1}O^{11}{}_{op}$
573				$2(\delta O^{14,11}C^{8,1}O^{15,13})_{oph}$
	564			CH_{2}twist (m) $+ \delta O^{9}C^{1}O^{12}{}_{op} + \delta C^{2}C^{5}{=}C^{6}{}_{op}$
			546	$\delta O^{12}C^{8}O^{13}{}_{ip} + \delta O^{10}C^{1}O^{11}{}_{op}$(w)
	522			CH_{2}twist (s) $+ \delta O^{9}C^{1}O^{12}{}_{op} + \delta C^{6}H^{7}{}_{op}$
			521	$\delta C^{6}{=}C^{5}C^{2}C^{1}{}_{(op)}$
502				CH_{2}rock $+ \delta C^{6}{=}C^{5}C^{2}$
	474			$\delta C^{5}{=}C^{6}{}_{op} + \delta O^{9}C^{1}O^{12}H^{13}{}_{ip}$
455				$\delta O^{15}C^{8}C^{6} + \delta O^{9}C^{5}{=}C^{6}$
			435	$\delta O^{13}C^{8}C^{6}{}_{ip} + \delta O^{9}C^{5}{=}C^{6}{}_{ip} + CH_{2}$rock(vw)

416			$\delta O^{13}C^{1}C^{2} + \delta O^{9}C^{5}\text{-}C^{2}$
	398		$\delta O^{11}C^{8}C^{6} + \delta O^{14}C^{5}{=}C^{6}$
		375	CH_2rock + $\delta C^{6}{=}C^{5}C^{2}$ (w)+ $\delta C^{5}{=}C^{6}C^{8}$ (vw)
	380		CH_2rock + $\delta O^{11}C^{8}C^{6} + \delta O^{14}C^{5}{=}C^{6}$

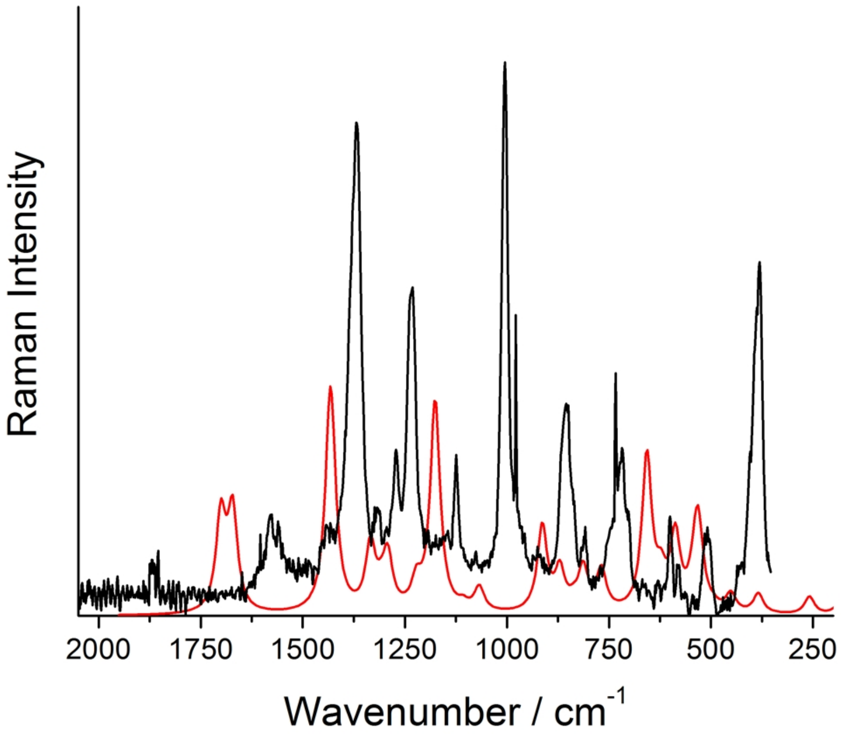

Figure S 10. Black: SERS spectrum of ket-AuNP. Red: Theoretical Raman spectrum of dicarboxyketone in ketone form.

One of the calculated Au-enol structures (Figure S 11), was not able to be optimized as a stable structure, leading to the products acetoacetate and carbon dioxide, as Turkevich and others suggested.[3,4] The main difference between the input of this species and the others is the fact that the whole enol is protonated and fully planar. In fact the final pHs of ket-AuNPs and cit-AuNPs synthesis are quite different (3.48 and 4.80 respectively), so, we believe the mechanism of functionalization is kinetically determined by the amount of citrate, its reactivity with temperature and by surface coordination.

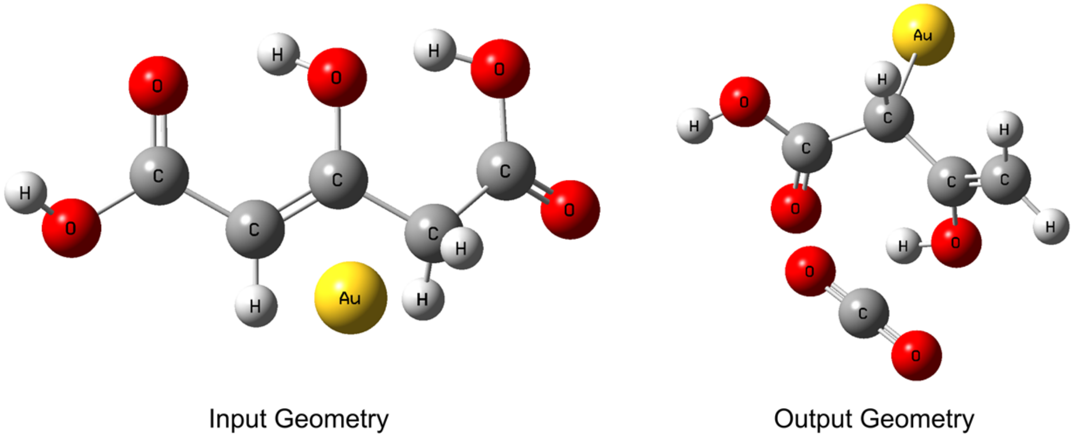

Figure S 11. Input and output geometries of dicarboxyketone in a protonated planar enol, showing the formation of acetoacetate and carbon dioxide after optimization.

For the Au_{20}-citrate (Figure S 12), the calculated electronic transitions showed more pronounced charge reorganization, rather than a charge transfer excitation as in the case of Au_{20}-enol. This charge delocalization represented by the blue/purple colors show almost no ligand participation in the transition and the band on the right is due to intracluster transitions[5].

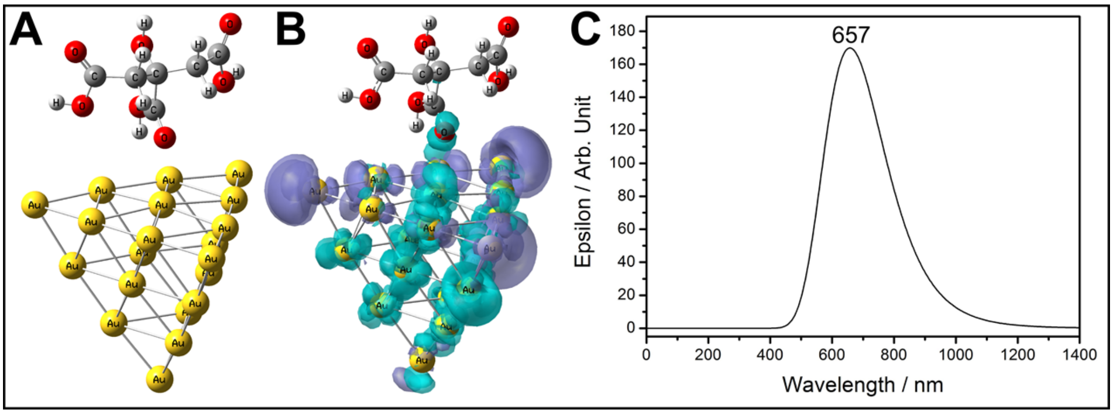

Figure S 12. A) Optimized structure B) Representation Charge Transfer state for the Au_{20}-Citrate system. The blue surfaces represents where the electrons are coming from and the purple surface represents where they are going. C) Electronic spectrum calculated by TD-DFT considering only the first three singlet states.

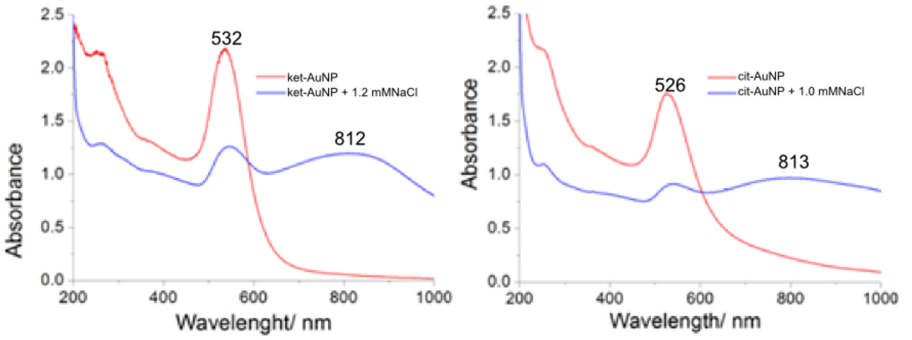

Figure S 13. Left: ket-AuNP, in red initial extinction spectra, in blue, extinction spectra with NaCl concentration of 1.2 mmolL^{-1}. Right: cit-AuNP, in red initial extinction spectra, in blue, extinction spectra with NaCl concentration of 1.0 mmolL^{-1}.

Reference

(1) Clayden, J.; Greeves, N.; Wrren, S.; Wothers, P. *Organic Chemistry*; Oxford: New York, **2007**; p. 1512.
(2) Yamamoto, S.; Watarai, H. *Langmuir* **2006**, *22*, 6562.
(3) Turkevich, J.; Stevenson, P. C.; Hillier, P. J. *Discuss. Faraday Soc.* **1951**, *11*.
(4) Munro, C. H.; Smith, W. E.; Garner, M.; Clarkson, J.; White, P. C. *Langmuir* **1995**, *11*, 3712.
(5) Sun, M.; Liu, S.; Chen, M.; Xu, H. *J. Raman Spectrosc.* **2009**, *40*, 137.